

## Dynamics of an array of mutually coupled semiconductor lasers

Serhiy Yanchuk,<sup>1,2,3,\*</sup> Andrzej Stefanski,<sup>4,†</sup> Tomasz Kapitaniak,<sup>4,‡</sup> and Jerzy Wojewoda<sup>4,§</sup>

<sup>1</sup>Weierstrass Institute for Applied Analysis and Stochastics, Mohrenstrasse 39, D-10117 Berlin, Germany

<sup>2</sup>Institute of Mathematics, Humboldt-University of Berlin, Unter den Linden 6, D-10099 Berlin, Germany

<sup>3</sup>Institute of Mathematics, National Academy of Sciences of Ukraine, Tereshchenkivska 3, 01601 Kiev, Ukraine

<sup>4</sup>Division of Dynamics, Technical University of Lodz, Stefanowskiego 1/15, 90-924 Lodz, Poland

(Received 25 April 2005; revised manuscript received 14 September 2005; published 12 January 2006)

We consider the dynamics of a linear array of coupled semiconductor lasers. Particular attention is paid to the synchronous states, which are caused by the permutation of two outer lasers. A system of three coupled lasers is studied in more details. We report different types of multistability of synchronous and asynchronous states including chaotic ones. We identify parameter values, for which a synchronous chaos can occur. Moreover, we show that transition to the synchronization occurs via blowup of the synchronous transversely unstable invariant set within the synchronization manifold. Finally, we present numerical analysis of larger arrays of coupled lasers and note some common qualitative features of the synchronization regions, which are independent of the number of lasers.

DOI: [10.1103/PhysRevE.73.016209](https://doi.org/10.1103/PhysRevE.73.016209)

PACS number(s): 05.45.Xt

### I. INTRODUCTION

The present paper is devoted to the theoretical study of a coupled semiconductor lasers array. The synchronization phenomena in coupled class *B* lasers have attracted a considerable attention during the last decades [1–16]. Among them, the papers [1–11] are dealing with coupled semiconductor lasers and [12–16] with the solid state lasers. We do not separate our analysis from the research for the solid-state lasers, since there are important similarities between these two types of lasers: both are class *B* lasers, since the polarization can be adiabatically eliminated. As a result, the dynamics of such systems can be described by the rate equations for complex electric field and inversion. At the same time, one should remember the principal differences between solid-state and semiconductor lasers, in particular, the linewidth enhancement factor ( $\alpha$  factor) for semiconductor lasers is much larger ( $\alpha \approx 3-5$ ) than for solid-state lasers ( $\alpha \approx 0$ ).

The dynamics of two coupled lasers was considered in [2–15,17]. Roy and Thornburg [13] performed experimental measurements and demonstrated synchronization of two neodymium: yttrium aluminum garnet (Nd:YAG) lasers, which are coupled via overlapping of the intracavity laser fields. Phase coherence properties of similar systems were studied in Refs. [12,14]. Ashwin *et al.* [15] showed that the loss of synchronization in two coupled class *B* lasers with a modulated loss can occur via blowout bifurcation. They showed also, that there exists a regime, for which the phases of the electric fields are synchronized while the amplitudes fluctuate nonsynchronously. For coupled semiconductor lasers with a short external cavity, a different regime was observed [11], for which the amplitudes are perfectly synchro-

nized while the phases are not. The case of a long external cavity was studied in Refs. [2,4], where the authors show the existence of symmetric, antisymmetric, and asymmetric solutions [2] and demonstrated lag synchronization phenomenon [4]. The effect of a parameter mismatch was studied in Ref. [3]. Lag synchronization in unidirectionally coupled semiconductor lasers was reported in Ref. [6] and the anti-synchronization of power dropouts in Ref. [17]. Peil *et al.* in Ref. [5] studied the influence of the relative feedback phase in the case of vectorial coupling on the dynamics of face-to-face coupled lasers. Other new phenomena were reported, such as retarded or anticipated synchronization [7,8,10,18], inverse synchronization [9], and localized synchronization [3].

Arrays of three coupled lasers were studied by Winful and Rahman [1] for the case of semiconductor lasers coupled by evanescent field, and by Terry *et al.* [16] for Nd:YAG lasers with either modulated pump or loss. In particular, paper [1] demonstrates the possibility of chaotic synchronization between the outer lasers in array, and Ref. [16] presents a detailed analysis of different symmetries, which occur in the array of three coupled identical lasers.

In the case when the external cavity of the linearly coupled lasers is short [11,16], the basic model for the study of the dynamics of the system can be formulated in terms of the instantaneously coupled (without delayed term) rate equations.

The purpose of the present paper is to study the synchronization properties of an array of three linearly coupled lasers with vectorial coupling, which is shown in Fig. 1. We provide conditions for the existence of stable synchronous states, where the key parameters are the injection phase shift (or distances between the lasers) and the coupling strength. We identify the parameter region, where a stable synchronous chaotic state exists. We also report about different types of coexistence of synchronous and asynchronous regimes. The presence of the injection phase parameter distinguishes our model from those considered in Refs. [1,16].

\*Email address: [yanchuk@wias-berlin.de](mailto:yanchuk@wias-berlin.de)

†Email address: [steve@p.lodz.pl](mailto:steve@p.lodz.pl)

‡Email address: [tomaszka@p.lodz.pl](mailto:tomaszka@p.lodz.pl)

§Email address: [wojewoda@p.lodz.pl](mailto:wojewoda@p.lodz.pl)

This paper is organized as follows. In Sec. II, we describe the mathematical model of the array of linearly coupled lasers. Synchronization of three coupled lasers is considered in Sec. III. Detailed bifurcation analysis in Sec. III A shows different types of multistability of synchronous and asynchronous regimes. A new mechanism of the transition to synchronization via blowup of the synchronous invariant set is identified and described in Sec. III B. Namely, we show that the blowup of the attractor within the synchronization manifold causes a change of its transverse stability properties. Discussion of the synchronization properties of an array of  $n$  coupled elements is presented in Sec. IV. We conclude about a similarity properties of the synchronization regions, which corresponds to the synchronization of the outer lasers. Finally, we conclude in Sec. V.

## II. THE MODEL

The schematic setup of the system under consideration is shown in Fig. 1. The equations, describing the dynamics of the slowly varying complex electric field amplitude  $E_i$  of the laser  $i$  is similar to that from Refs. [13,16,19]. It is the coupled rate equations

$$\begin{aligned} \frac{dE_1}{dt} &= \frac{1}{2} \left( \mathcal{G}_1(N_1, |E_1|^2) - \frac{1}{\tau_{p_1}} \right) E_1 + \kappa e^{-i\varphi} E_2, \\ \frac{dN_1}{dt} &= I_1 - \frac{N_1}{\tau_{c_1}} - \text{Re}[\mathcal{G}_1(N_1, |E_1|^2)] |E_1|^2, \\ \frac{dE_2}{dt} &= \frac{1}{2} \left( \mathcal{G}_2(N_2, |E_2|^2) - \frac{1}{\tau_{p_2}} \right) E_2 + \kappa e^{-i\varphi} (E_1 + E_3), \\ \frac{dN_2}{dt} &= I_2 - \frac{N_2}{\tau_{c_2}} - \text{Re}[\mathcal{G}_2(N_2, |E_2|^2)] |E_2|^2, \\ &\dots \\ \frac{dE_n}{dt} &= \frac{1}{2} \left( \mathcal{G}_n(N_n, |E_n|^2) - \frac{1}{\tau_{p_n}} \right) E_n + \kappa e^{-i\varphi} E_{n-1}, \\ \frac{dN_n}{dt} &= I_n - \frac{N_n}{\tau_{c_n}} - \text{Re}[\mathcal{G}_n(N_n, |E_n|^2)] |E_n|^2, \end{aligned} \quad (1)$$

where  $E_j$  and  $N_j$  denote the complex optical fields and the carrier densities of the lasers, respectively. By  $I_j$ , we denote the pumping current, and  $\mathcal{G}_j(N_j, |E_j|^2)$  is the complex gain function.  $\tau_{p_j}$ ,  $\tau_{c_j}$  are photon and carrier lifetimes;  $\kappa$  characterizes the injection rate. We assumed in (1) that there is no detuning between the lasers. Moreover, in the following, we assume that the lasers are identical. Note that the model (1) is also valid for the case of coupling by evanescent field if we fix  $\varphi = -\pi/2$ , cf. [1]. We introduce the following simplifications and rescalings. Neglecting nonlinear gain saturation, we linearize the complex gain function as follows:

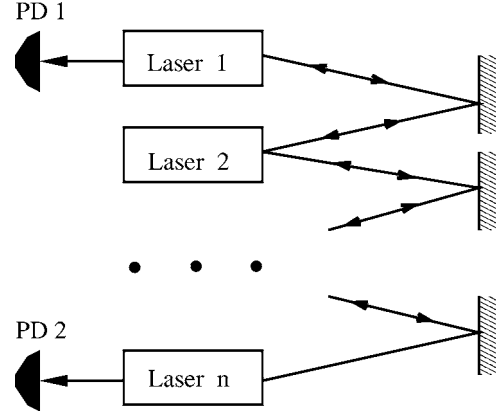


FIG. 1. Schematic representation of the array of linearly coupled lasers. PD1 and PD2 are the photodiodes, which detect the output from the outer lasers.

$$\mathcal{G}(N, |E|^2) - \frac{1}{\tau_p} := G_N(1 + i\alpha)(N - N_0).$$

With the rescaling  $E_{\text{new}} = \sqrt{G_N \tau_c / 2} E$ ,  $N_{\text{new}} = \frac{1}{2} \tau_p G_N (N - N_0)$ ,  $t_{\text{new}} = t / \tau_p$ , we obtain the following system:

$$\begin{aligned} E'_1 &= (1 + i\alpha) N_1 E_1 + \eta e^{-i\varphi} E_2, \\ N'_1 &= \varepsilon [J - N_1 - (2N_1 + 1) |E_1|^2], \\ E'_j &= (1 + i\alpha) N_j E_j + \eta e^{-i\varphi} (E_{j-1} + E_{j+1}), \\ N'_j &= \varepsilon [J - N_j - (2N_j + 1) |E_j|^2], \quad j = 2, \dots, n-1, \\ E'_n &= (1 + i\alpha) N_n E_n + \eta e^{-i\varphi} E_{n-1}, \\ N'_n &= \varepsilon [J - N_n - (2N_n + 1) |E_n|^2], \end{aligned} \quad (2)$$

where we use the same notations for the new variables. The differentiation is assumed to be made with respect to the new time, and the parameters are

$$\eta = \tau_p \kappa, \quad \varepsilon = \tau_p / \tau_c, \quad J = \tau_p G_N (I \tau_c - N_0) / 2.$$

Note, that the phase-shift invariance  $(E_j, N_j) \rightarrow (E_j e^{i\psi}, N_j)$  of system (2) implies, that for suitable laser parameters there exist compound cavity modes, i.e., solutions of the type  $E_j(t) = E_0 e^{i\omega t}$ ,  $N_j = N_0$  ( $j = 1, \dots, n$ ;  $\omega \in \mathbb{R}$ ). These solutions will be called “stationary,” because they correspond to stationary intensity regimes.

In Sec. III, we consider the case of three coupled lasers.

## III. THREE COUPLED LASERS

### A. Regions of different synchronization types

The case of three coupled lasers has been already studied in some details in Refs. [1,16]. Note that the experimental setup from Ref. [16] leads to the confinement  $\varphi = \pi$ . As it will follow from our analysis (cf. Fig. 2), the preferable dynamics of the systems in this case is stationary unless some

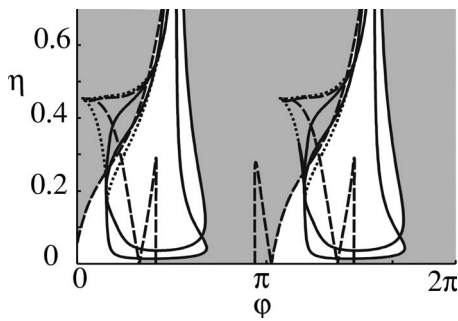


FIG. 2. Two-dimensional bifurcation diagram for the stability of stationary states within the manifold  $M_s$ . The gray shaded regions show the parameter values, for which there exists a stable stationary state. Solid lines denote Hopf bifurcations, dotted lines, the fold bifurcations, and broken lines the pitchfork bifurcations. Fixed parameters are  $\alpha=2, J=1, \varepsilon=0.03$ .

additional destabilization mechanism is present. Such an additional mechanism in Ref. [16] was a periodic modulation of the pump or losses. The setup from Ref. [1] leads to  $\varphi = -\pi/2$  and, as a result, the authors were able to find the regime of synchronous chaos. In the following, we will study the influence of feedback phase  $\varphi$  on the dynamics of the system in some details.

The question about symmetries in the model of three coupled lasers has been addressed in Ref. [16]. Therefore, we will not study here the symmetries in details. Nevertheless, it is important for our study to mention that, due to the coupling configuration, there is no possibility to synchronize an outer laser with the middle one, i.e., the manifold  $E_1=E_2, N_1=N_2$  is not invariant with respect to (2). Instead, the six-dimensional manifold  $M_s=\{E_1=E_3, N_1=N_3\}$ , which corresponds to the synchronization of outer lasers, is invariant.

We perform a stability analysis of the manifold  $M_s$ . First, we present the two-dimensional bifurcation diagram for the stability of stationary states in Fig. 2. One can identify different bifurcations: Hopf, fold, and pitchfork, which lead to the destabilization of synchronous stationary states [20]. The shaded regions correspond to the parameter values, for which there exists a stable state.

Note, that Fig. 2 reveals the local stability properties of the synchronous stationary states. In order to have an insight to the transverse stability of the whole manifold  $M_s$ , we perform also a numerical analysis and show results in Fig. 3. A grid  $100 \times 100$  was introduced to discretize a square region of the parameter  $\eta$  and  $\varphi$  values. From each obtained cell, we have chosen a pair of parameters  $\varphi, \eta$ , for which an orbit was computed starting from some initial condition near the manifold but not exactly symmetric. The gray areas show the regions, for which the orbit was attracted to the manifold, i.e., for which it was synchronized.

One can conclude, comparing Figs. 2 and 3, that the stationary synchronization dominates among all possible synchronization regimes. The difference in sizes of the shaded regions in Figs. 2 and 3 indicate that there is a coexistence of the synchronous and nonsynchronous regimes. In addition, one can find parameter values, where periodic or chaotic synchronization takes place. The detailed one-dimensional bifurcation diagrams for  $\varphi = \pi/2$  in Fig. 4 reveals these re-

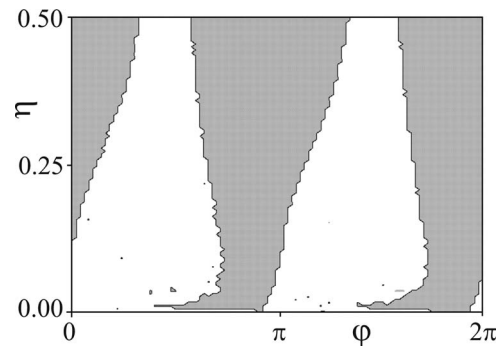


FIG. 3. Numerically obtained parameter region for the stability of the synchronization manifold  $M_s$ .

gimes. Comparing the bifurcation diagrams (a) and (b) in Fig. 4, we can see that for  $0 < \eta < 0.0156$ , a stable critical point is an attractor of the system and stationary synchronization occurs. As a result of Hopf bifurcation at  $\eta=0.0156$ , a limit cycle within the manifold  $M_s$  appears, but the synchronized state is still retained. Periodic synchronization loses its stability at  $\eta=0.022$  via transverse Hopf bifurcation even though the limit cycle on the synchronization manifold is still stable. Further increase of parameter  $\eta$  leads to the appearance of a chaotic invariant set within the synchronization manifold via a cascade of period doubling bifurcations at  $\eta=0.0275$ . This set becomes again transversely stable at  $\eta=0.0284$  implying chaotic synchronization. For some narrow range around  $\eta \approx 0.03$  (see Fig. 5), a coexistence of the synchronous and asynchronous attractors in the phase space occurs. When parameter  $\eta$  increases, the asynchronous attractor becomes chaotic via period-doubling [Fig. 5(b)] bifurcations. This multistability can be observed for  $0.0284$

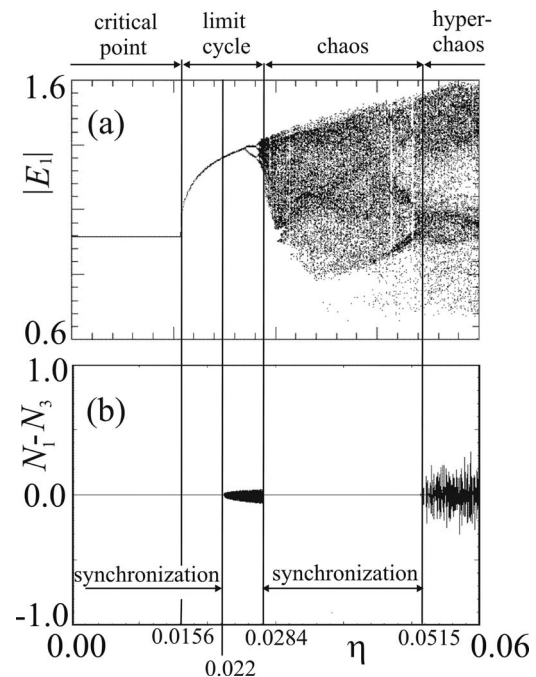


FIG. 4. One-dimensional bifurcation diagram of the synchronous system attractor (a) and corresponding ranges of synchronization (b).  $\varphi = \pi/2$  is fixed.

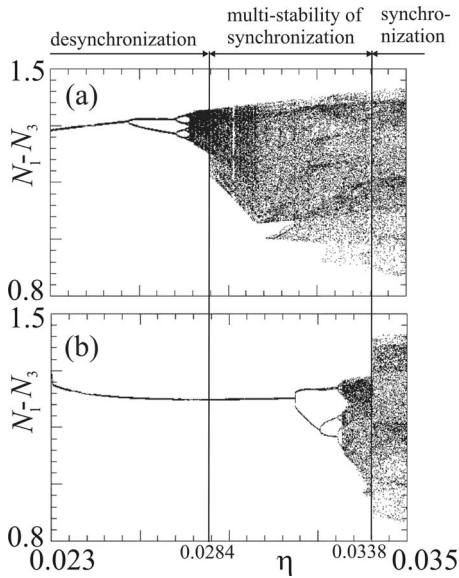


FIG. 5. Bifurcation diagrams for synchronous (a) and asynchronous (b) attractors. Zoom of the interval  $0.022 < \eta < 0.035$ . The region of multistability is indicated.

$< \eta < 0.0338$ . The asynchronous solution becomes unstable and stable chaotic synchronization is dominant for  $0.0338 < \eta < 0.0515$ , since at  $\eta = 0.0515$  the chaotic attractor loses its stability. The new asynchronous attractor can be shown to be hyperchaotic, because its spectrum of Lyapunov exponents contains two positive exponents ( $\lambda_1 = 0.0442$  and  $\lambda_2 = 0.0035$  for  $\eta = 0.052$ ).

A confirmation of the observations described above is given in Fig. 6. This figure shows behavior of Lyapunov exponents for the manifold  $M_s$ . One observes the following points, where the behavior changes qualitatively: A is a transverse Hopf bifurcation. As a result of this bifurcation, a

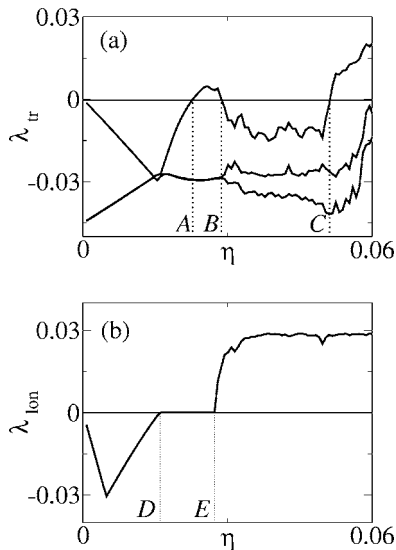


FIG. 6. Behavior of the Lyapunov exponents. (a) Transverse Lyapunov exponents and (b) the largest longitudinal Lyapunov exponent. The parameters are the same as in Fig. 4. Bifurcation points A–E are explained in the text.

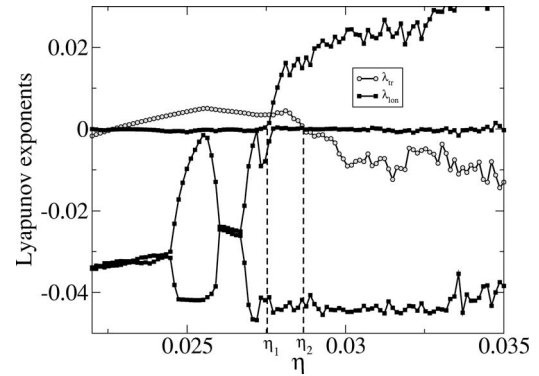


FIG. 7. Lyapunov exponents. Zoom of the interval  $0.022 < \eta < 0.035$ .

stable periodic solution appears, which is not located in the manifold  $M_s$ . At a point B, the chaotic attractor in the manifold  $M_s$  becomes stable. It loses its stability at the point C. Therefore, we have a stationary synchronization for  $0 < \eta < 0.0156$ , periodic synchronization for  $0.0156 < \eta < 0.022$ , and chaotic for  $0.0284 < \eta < 0.0515$ .

Section III B studies, in some detail, the transition to the chaotic synchronization, since it seems to contain different features compared with known mechanisms of synchronization, see, for example, Refs. [21,22].

### B. Transition to chaotic synchronization via blowup of a transversely unstable synchronous invariant set

Let us consider, in detail, the mechanism of the synchronization for parameter values  $\eta \approx 0.028$ , cf. Fig. 4. One can observe that shortly after the synchronous attractor becomes chaotic at  $\eta_1 = 0.0275$ , it becomes transversely stable at  $\eta_2 = 0.0284$ , cf. Figs. 7 and 5.

As follows from the bifurcation diagram in Fig. 5, at the moment when the synchronous attractor becomes transversely stable at  $\eta_2 = 0.0284$ , it undergoes a blowup, i.e., the size of the attractor rapidly increases. The coincidence of these two effects seems not to be occasional. First, we suggest an explanation, which is based on the concept of local Lyapunov exponents [23]. Figure 8 shows regions within the chaotic attractors, which are transversely stable. Namely, we computed the local contraction and/or expansion ratio by means of the local transverse Lyapunov exponents

$$\lambda_{loc}^{(i)} = 1/T \ln |\mu_i(\Phi(T, x))|, \quad i = 1, 2, 3,$$

where  $\Phi(T, x)$  is the fundamental matrix corresponding to the linearized dynamics of the transverse perturbations,  $\mu_i(\dots)$  is an  $i$ th eigenvalue of a matrix.  $\Phi(T, x)$  depends on the integration interval, which is chosen to be small in our case ( $T = 1.0$ ) in order to reveal the local expansion properties, and  $x$ , which is a point on the synchronous attractor. We estimated numerically  $\lambda_{loc}^{(i)}$  and marked in Fig. 8, those points on the attractor, which produce all  $\lambda_{loc}^{(i)}$  negative. This method allows us to find transversely attracting regions on the attractor. The final transverse stability is then deduced from the averaging over the whole attractor. It can be seen that the major part of the attractor after the blowup in Fig. 8 is cov-

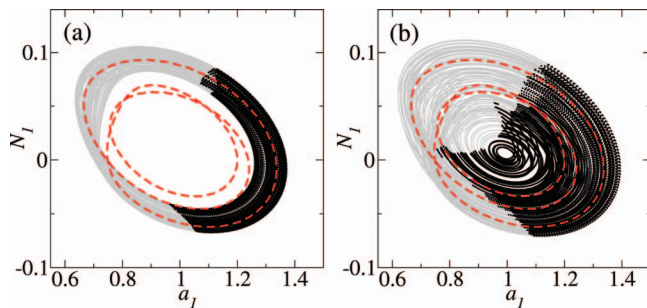


FIG. 8. (Color) The phase portraits [projection onto the  $(a_1 = |E_1|, N_1)$  plane] of the synchronous attractor before the blowup (a) at  $\eta=0.0282$  and after (b) at  $\eta=0.0287$ . Those parts of the attractors which possess negative local Lyapunov exponents are marked by the black points. Period-3 unstable periodic orbit is shown by broken line (red).

ered by transversely stable points, i.e., the “new” part of the attractor brings additional transverse stability. This fact allows us to assume that the blowup of the attractor corresponds to its transverse stabilization as well.

We would like to clarify the underlying bifurcation mechanisms, which cause the observed phenomenon to occur. The inspection of the system dynamics and the continuation technique [24] reveal that the blowup of the synchronous attractor at  $\eta=0.0284$  occurs via a collision with a chaotic saddle. The chaotic saddle is located in the phase space as shown in Fig. 9(b). In order to detect the geometrical place of this unstable chaotic saddle, we used the continuation technique. We followed the unstable low-periodic orbits, which were born in the period-doubling cascade.

In the following, for the brevity we will use notations:  $\mathcal{A}$  for the synchronous chaotic attractor (e.g., in Fig. 8); CS for the chaotic saddle [e.g., in Fig. 9(b)].

Figure 9(a) shows the main bifurcation branch, which leads to the appearance of the CS. Particularly, at  $\eta=0.02762$  (LP point in the figure), a pair of period-3 orbits appears [25] via a fold bifurcation. The branch with the smaller period leads then to the period-doubling bifurcation at  $\eta=0.02783$  (PD), where period-6 orbit is created. We were able to follow a few consecutive period-doubling bifur-

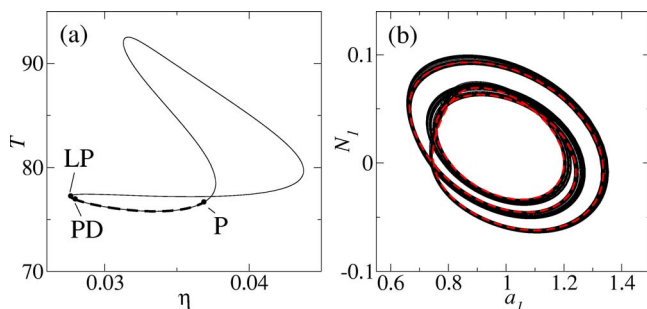


FIG. 9. (Color online) (a) The bifurcation diagram for the period-3 unstable periodic orbit. LP—fold bifurcation ( $\eta=0.02762$ ), PD—period-doubling bifurcation ( $\eta=0.02783$ ).  $T$  denotes the actual period of the orbit. (b) The three-band chaotic saddle (CS), which is created through the period-doubling cascade of period-3 orbit (broken line, red online) at  $\eta=0.0280$ .

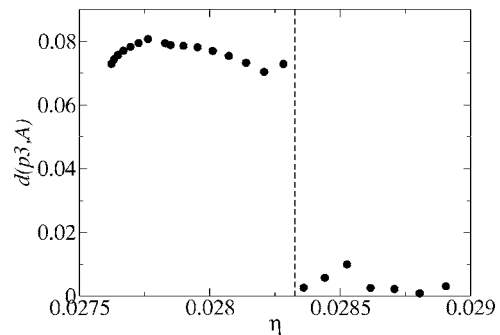


FIG. 10. Distance between the synchronous attractor  $\mathcal{A}$  and the period-3 orbit, which is embedded in the chaotic saddle. At  $\eta=0.0284$ , the distance rapidly decreases indicating that the period-3 orbit becomes a part of the attractor with increasing  $\eta$ .

cations, which apparently lead to the appearance of three-band CS in the vicinity of the period-3 orbit. We also found that this set is stable with respect to transverse perturbations. Since CS is unstable longitudinally, we observe the following scenario: when the system starts close to the CS, it undergoes a relatively long synchronous transient along the CS and then approaches the longitudinally stable chaotic set  $\mathcal{A}$ . Afterward, it is repelled in the transverse direction exhibiting desynchronization.

The collision of the sets CS and  $\mathcal{A}$  occurs at  $\eta=0.0284$ , producing a larger attractor. Although this collision can already be observed from Fig. 8, this is not enough to prove this fact, since Fig. 8 gives only the projection. A more correct proof is given in Fig. 10, where the distance  $d(\mathcal{A}, p3)$  between the attractor  $\mathcal{A}$  and the period-3 orbit embedded in the CS is plotted. More exactly, we define

$$d(\mathcal{A}, p3) = \inf_{t_1 \in [0, T_1]; t_2 \in [0, T_2]} |x(t_1) - y(t_2)|,$$

where  $x(t_1)$  is the period-3 orbit with the actual period  $T_1$  and  $y(t_2)$  is the orbit on the attractor  $\mathcal{A}$  of large enough length  $T_2$ . In our simulations, we used  $T_2=5 \times 10^4$ . We clearly observe the transition at  $\eta=0.0284$  when the period-3 orbit becomes a part of a synchronous attractor. Small deviations from zero for  $\eta>0.0284$  are resulted from finiteness of  $T_2$ .

#### IV. ARRAYS OF COUPLED OSCILLATORS

Having computed the bifurcation diagram in Fig. 2 and numerical study of the stability of synchronous state in the system of three coupled lasers in Fig. 3, one can compare it with the similar stability analysis for two face-to-face coupled lasers, cf. Fig. 1 in Ref. [11]. The qualitative similarity of the results is evident. In the both cases, there are two large regions of the synchronization of outer lasers, which are located near  $\varphi \approx 0$  and  $\varphi \approx \pi$ .

In order to check the universality of this observation, we computed numerically similar synchronization diagrams for larger arrays. The results are shown in Fig. 11 for five and ten oscillators. One can recognize the same qualitative trend. Note, that the synchronization considered here corresponds only to the asymptotic coincidence of the variables of the

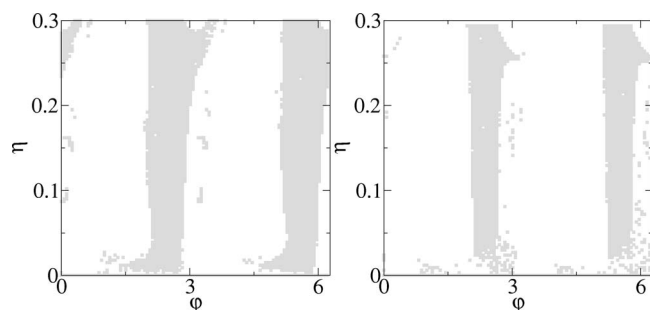


FIG. 11. The regions in the  $\varphi$ - $\eta$  parameter space, for which an orbit started from randomly chosen initial condition is attracted to the synchronization manifold  $M_s$ . This corresponds to the asymptotic synchronization of the outer lasers. (a) Five coupled lasers, (b) ten coupled lasers.

outer lasers, i.e.,  $E_n = E_1$ ,  $N_n = N_1$ . This is not necessary for the complete synchronization of the whole array. In general, the synchronization of outer lasers may include some cluster states as well, cf. Refs. [26,27]. Figure 11 has been obtained by computing asymptotic behavior of orbits started from randomly chosen initial conditions.

## V. CONCLUSIONS

We have studied the dynamical behavior of the linear array of coupled semiconductor lasers. Detailed analysis was focused on the stability of synchronous and asynchronous states, both regular and chaotic of the array of three lasers. We identified the mechanism of the transition in which the

synchronous state appears via blowup bifurcation of the attractor within the synchronization manifold. Finally, we discussed possibility of generalization of our results to the case of  $n$ -coupled lasers. It has been shown that some qualitative features of the synchronization regions are independent on the number of lasers.

We note that the considered model corresponds to the ideal case when all lasers are identical. In a realistic situation, one can imagine that the parameters of the systems as well as feedback phases can be slightly different. In this case, we expect that the results presented in Fig. 2 should be robust to the mismatch because of the following reason: The regions depicted in the figure correspond to the asymptotic stability of stationary states and, as it is known from the general theory, this property is robust under small parameter mismatches.

Similarly, the corresponding results are true for sufficiently small delay in the coupling. Moreover, the study of the delay influence in the case of two coupled lasers [11] suggests that the effect of a small delay will result in slight changing of slopes of the corresponding bifurcation lines in Fig. 2, while the qualitative features will remain the same. We refer to Ref. [11] for more detailed discussion of the influence of delay in a similar type of model.

## ACKNOWLEDGMENTS

S.Y. was supported by DFG (Sonderforschungsbereich 555 ‘‘Komplexe nichtlineare Prozesse’’). A.S., T.K., and J.W. were supported by the Polish Department for Scientific Research (DBN) under Project No. 4 T07A 044 28.

- 
- [1] H. G. Winful and L. Rahman, *Phys. Rev. Lett.* **65**, 1575 (1990).
  - [2] J. Javaloyes, P. Mandel, and D. Pieroux, *Phys. Rev. E* **67**, 036201 (2003).
  - [3] A. Hohl, A. Gavrielides, T. Erneux, and V. Kovanis, *Phys. Rev. Lett.* **78**, 4745 (1997).
  - [4] T. Heil, I. Fischer, W. Elsäßer, J. Mulet, and C. R. Mirasso, *Phys. Rev. Lett.* **86**, 795 (2001).
  - [5] M. Peil, T. Heil, I. Fischer, and W. Elsäßer, *Phys. Rev. Lett.* **88**, 174101 (2002).
  - [6] I. V. Koryukin and P. Mandel, *Phys. Rev. E* **65**, 026201 (2002).
  - [7] C. Masoller, *Phys. Rev. Lett.* **86**, 2782 (2001).
  - [8] E. M. Shahverdiev, S. Sivaprakasam, and K. A. Shore, *Phys. Rev. E* **66**, 017206 (2002).
  - [9] S. Sivaprakasam, I. Pierce, P. Rees, P. S. Spencer, K. A. Shore, and A. Valle, *Phys. Rev. A* **64**, 013805 (2001).
  - [10] J. K. White, M. Matus, and J. V. Moloney, *Phys. Rev. E* **65**, 036229 (2002).
  - [11] S. Yanchuk, K. R. Schneider, and L. Recke, *Phys. Rev. E* **69**, 056221 (2004).
  - [12] L. Fabiny, P. Colet, R. Roy, and D. Lenstra, *Phys. Rev. A* **47**, 4287 (1993).
  - [13] R. Roy and K. S. Thornburg, *Phys. Rev. Lett.* **72**, 2009 (1994).
  - [14] K. S. Thornburg, M. Möller, R. Roy, T. W. Carr, R. D. Li, and T. Erneux, *Phys. Rev. E* **55**, 3865 (1997).
  - [15] P. Ashwin, J. R. Terry, K. S. Thornburg, and R. Roy, *Phys. Rev. E* **58**, 7186 (1998).
  - [16] J. R. Terry, K. S. Thornburg, D. J. DeShazer, G. D. Vanwiggeren, S. Zhu, P. Ashwin, and R. Roy, *Phys. Rev. E* **59**, 4036 (1999).
  - [17] I. Wedekind and U. Parlitz, *Phys. Rev. E* **66**, 026218 (2002).
  - [18] H. U. Voss, *Phys. Rev. E* **61**, 5115 (2000).
  - [19] S. Yanchuk, K. R. Schneider, and L. Recke, *Proc. SPIE* **5452**, 51 (2004).
  - [20] The branches of bifurcations have been obtained by the continuation software *CONTENT* [24].
  - [21] S. Yanchuk, Y. Maistrenko, and E. Mosekilde, *Physica D* **154**, 26 (2001).
  - [22] S. Yanchuk, Y. Maistrenko, and E. Mosekilde, *Chaos* **13**, 388 (2003).
  - [23] N. F. Rulkov and M. M. Sushchik, *Int. J. Bifurcation Chaos Appl. Sci. Eng.* **7**, 625 (1997).
  - [24] Yu. A. Kuznetsov and V. V. Levitin, *CONTENT: A Multiplatform Environment for Continuation and Bifurcation Analysis of Dynamical Systems* (Centrum voor Wiskunde en Informatica, Amsterdam, 1997).

- [25] The orbits, which rotate  $n$  times around some rotation center, are usually called period- $n$  orbits, since they correspond to period- $n$  cycles of the corresponding Poincaré map.
- [26] M. Golubitsky and I. Stewart, in *Equadiff 2003: Proceedings of the International Conference on Differential Equations*, edited by F. Dumortier, H. Broer, J. Mawhin, A. Vanderbauwhede, and S. V. Lunel (World Scientific, Singapore, 2005), pp. 13–24.
- [27] M. Golubitsky, I. Stewart, and A. Torok, *SIAM J. Appl. Dyn. Syst.* **4**, 78 (2005).